



## Analysis of Heat Transfer of Ribbed Turbulent Channel using ANSYS

Mayank Bhola

Assistant Professor Department of Mechanical Engineering,  
Amrapali Group of Institutes, Haldwani, (Uttarakhand), India

**ABSTRACT:** This paper presents the 2-D numerical simulation for heat transfer and friction factor characteristics of ribbed turbulent channel, with bottom plate applied to constant flux thermal boundary condition, and upper plate is insulated. The fluid domain is designed using ANSYS Workbench software and simulated using ANSYS Fluent software, based on finite element method. Parameters like Nusselt number, friction factor and heat transfer coefficient have been obtained for the design, and contours of temperature and velocity are presented. The groove length/rib length (B) to channel height (H) ratios are taken as 0.5, 0.75, 1.0 for the geometry. The main objective of the work performed was to find the best B/H ratio under similar boundary conditions.

**Keywords:** Turbulent channel, ANSYS, 2-D Analysis, Ribbed geometry, Realizable k- turbulence model

### I. INTRODUCTION

In recent years many researchers have contributed for enhancing heat transfer characteristics of parallel plate heat exchanger with one plate insulated and other subjected to constant flux thermal boundary condition. Luo et al. (2004) conducted experimental studies to examine the force convection and flow friction characteristics of fully developed turbulent flow in air cooled horizontal equilateral triangular duct with internal surface fabricated with uniformly spaced square ribs. They studied the effect of duct geometry as well as Reynolds no. on the test rig, and determined the optimum relative rib height and relative rib to rib spacing corresponding to maximum thermal performance. Sahu and Gandhi (2014) numerically investigated the effect on heat transfer and flow field characteristics due to an inclined rib with a gap on solar air heater duct. They determined that Realizable k- turbulence model with standard wall function provides best result for these kind of problems to be solved numerically. Tatsumi *et al.* (2002) conducted a 3-D numerical computation for determining flow and thermal fields over full-span and discrete array of rib attached to a channel with 90° inclination against the flow direction. They predicted that generation of vortices is effective to reduce the area of the flow recirculation region and is effective to increase the wall heat transfer. Vijiapurapu and Cui (2007) simulated turbulent flow in a ribbed pipe using large eddy simulation. The spacing between the ribs is varied to

form three representative types of surface roughness: d-type, intermediate, and k-type. It has been noted that both intermediate- and k-type roughness produce strong roughness effects with dominant pressure resistance, but the flows with different types of surface roughness exhibit quite different characteristics in terms of mean flow quantities and coherent eddy structures. Singh and Singh (2014) performed a numerical analysis of heat transfer in turbulent channel flow using triangular winglet type longitudinal vortex generator of different angle at Reynolds number 10,000. They observed that heat transfer increases with increase in angle of attack for same Reynolds number. And conclude increase of pumping power to flow fluid through the channel. Mashilkar and Varkute (2014) conducted a 3-D computational analysis of heat transfer augmentation and flow characteristics due to three different artificial roughness geometries in form of turbulators, pin-fin and conical fins on heated wall of rectangular solar air heater duct. They used Realizable k- turbulence model with enhanced wall treatment for capturing physics at near wall. Kumar and Agarwal (2014) also conducted a CFD analysis to determine effect on heat transfer coefficient and friction factor due to rectangular ribs on rectangular duct of solar air heater. Effect of trapezoidal ribs on heat transfer coefficient of absorber plate of solar air heater used for low temperature heating purpose, and agriculture drying purpose was studied by Singh and Bartaria (2013). They concluded that by imposed artificial roughness friction factor also increases with increase in Nusselt number. Sohankar

(2010) conducted a simulation to determine the fluid flow and heat transfer characteristics through a rib-roughened duct of square cross-section, he used SIMPLEC algorithm to couple pressure and velocity in the solution. He concluded that, though augmentation increases the heat transfer but the constant turbulent Prandtl number of the turbulent model used also has a significant effect on the simulation results of heat transfer. Deylami *et al.* (2013) conducted a numerical investigation to study the effect of corrugation on heat transfer and pressure drop in a corrugated channel. They made the changes in rib-height to channel-height and also there concern was to find adequate turbulence model for numerical solution. Bhola and Singh (2015) numerically investigated the experiments of Lorenz *et al.* (1995) using Realizable K- turbulent model and results were found close to the results of Eiamsa-ard and Promvong (2008) for grooved turbulent channel. In the present research, numerical investigation of 2-D ribbed turbulent channel is conducted to verify the suitable B/H ratio for better heat transfer for such geometry.

## II. GEOMETRY OF THE PRESENT PROBLEM

The geometry created for analysis was made of aluminum of 0.68 m length and has hydraulic diameter of 0.08 m in which air flow occurs. Protrusions made on plate were rib with 9 ribs. These geometries are used for studying the effects of the variation of geometries on the performance of plate heat exchanger. Value of “S” will change according to the variations in “B”. The dimension of the constant heat flux test section mentioned above is the same as the grooved channel of Eiamsa-ard and Promvong [4], but instead of grooves, rib protrusions are used.

A uniform rectangular mesh is used to resolve the laminar sub-layer. To obtain grid independence solution, number of cells is varied between 55,000 and 158,000 meshes. The mean inlet velocity between 1.19 and 2.19 m/s is based on Reynolds number cited above, zero pressure gradients at the exit and no slip wall boundary conditions are taken for the present computation. In previous research, Chaube *et al.* [2] suggested that the calculation with 2- dimensional flow model yields the results closer to measurements as compared that with 3-dimensional flow. In this work, the 2D flow is therefore carried out for saving computer memory and computational time.

**Table 1: Geometric description of model.**

Total length (m)	1.88
Entry length (m)	0.8
Length of test section (m)	0.68
Exit length (m)	0.4
Rib height (e), (m)	0.02
Rib length (B), (m)	0.02, 0.03, 0.04
Distance between two plates (H), (m)	0.04
Length of period (P), (m)	0.08

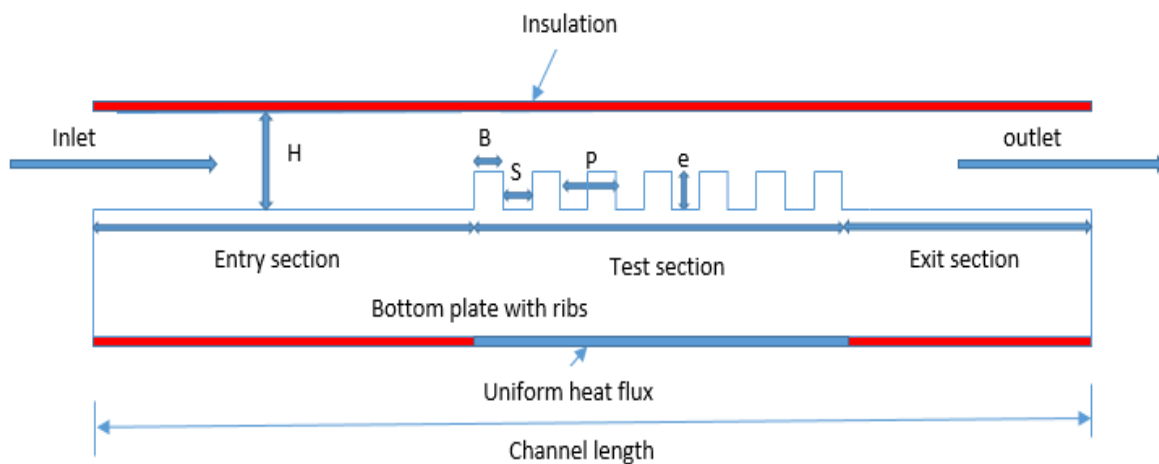


**Fig. 1.** Schematic diagram for channel flow configuration.

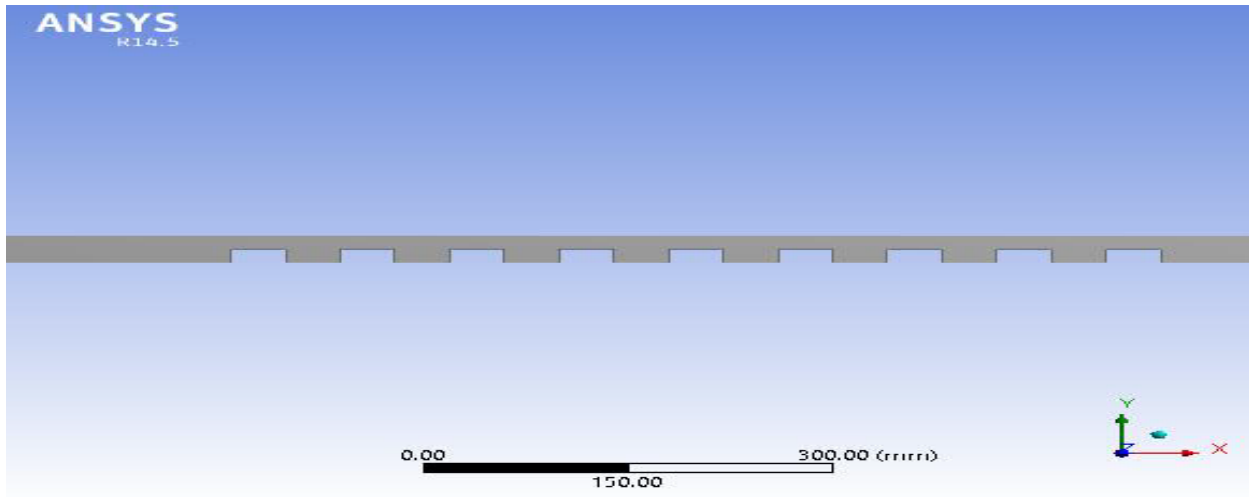


Fig. 2. Geometry of ribbed channel.

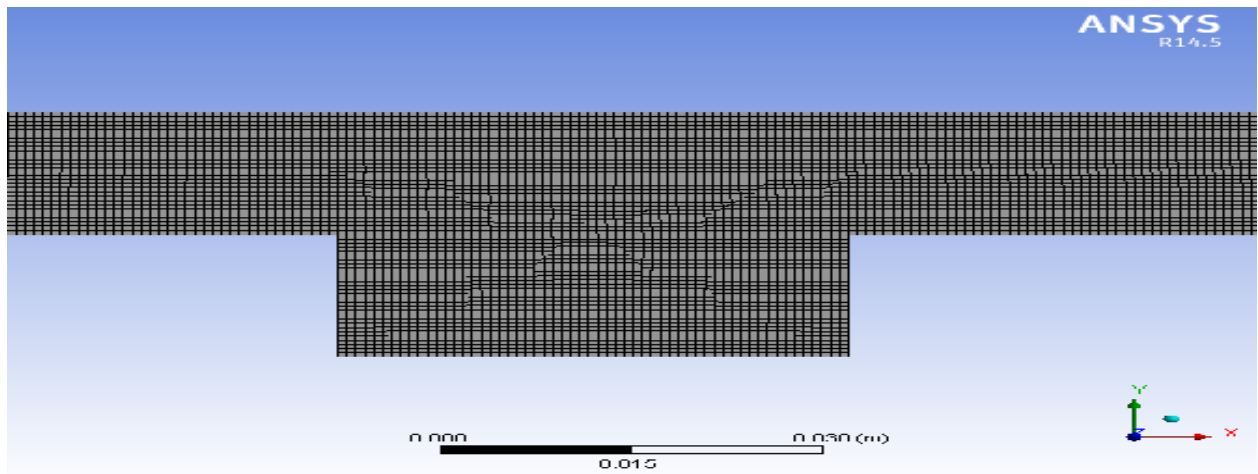


Fig. 3. Mesh generation of Ribbed Channel.

### III. MATHEMATICAL MODELING

The fluid domain under consideration is governed by the steady 2- Dimensional form of the continuity, the time-averaged incompressible Navier–Stokes equations and the energy equation. These equations can be written as:

A. Continuity equation

$$\frac{\delta(\rho\bar{u})}{\delta x} + \frac{1}{r} \frac{\delta(\rho r\bar{v})}{\delta r} = 0$$

B. Momentum equation

Axial component

$$\rho\bar{v} \left[ \frac{\delta\bar{u}}{\delta r} + \bar{u} \frac{\delta\bar{u}}{\delta x} \right] = \frac{\delta\bar{p}}{\delta x} + \frac{\delta}{\delta x} \left( \mu_{eff} \frac{\delta\bar{u}}{\delta x} \right) + \frac{1}{r} \frac{\delta}{\delta r} \left( \mu_{eff} \frac{\delta\bar{u}}{\delta r} \right) + \frac{\delta}{\delta x} \left( \mu_{eff} \frac{\delta\bar{u}}{\delta x} \right) + \frac{1}{r} \frac{\delta}{\delta r} \left( \mu_{eff} \frac{\delta\bar{u}}{\delta r} \right)$$

Radial component

$$\rho \left[ \bar{v} \frac{\delta\bar{v}}{\delta r} + \bar{u} \frac{\delta\bar{v}}{\delta x} \right] = -\frac{\delta\bar{p}}{\delta r} + \frac{\delta}{\delta x} \left( \mu_{eff} \frac{\delta\bar{v}}{\delta x} \right) + \frac{1}{r} \frac{\delta}{\delta r} \left( r\mu_{eff} \frac{\delta\bar{v}}{\delta r} \right) + \frac{\delta}{\delta x} \left( \mu_{eff} \frac{\delta\bar{v}}{\delta x} \right) + \frac{1}{r} \frac{\delta}{\delta r} \left( r\mu_{eff} \frac{\delta\bar{v}}{\delta r} \right) - 2\mu_{eff} \frac{\bar{v}}{r^2} + \rho \frac{\bar{w}^2}{r}$$

Tangential component

$$\rho \left[ \bar{v} \frac{\delta \phi}{\delta r} + \bar{u} \frac{\delta \phi}{\delta x} \right] = \frac{\delta}{\delta z} \left[ \mu_{eff} \frac{\delta \phi}{\delta x} \right] + \frac{1}{r} \frac{\delta}{\delta r} \left[ r \mu_{eff} \frac{\delta \phi}{\delta r} \right] - \frac{2}{r} \frac{\delta}{\delta r} \left[ \mu_{eff} \phi \right]$$

C. Energy equation

$$\rho_{Dt}^{DE} = -div(pu) + \left[ \frac{\partial(u\tau_{xx})}{\partial x} + \frac{\partial(u\tau_{yx})}{\partial y} + \frac{\partial(u\tau_{zx})}{\partial z} + \frac{\partial(v\tau_{xy})}{\partial x} + \frac{\partial(v\tau_{yy})}{\partial y} + \frac{\partial(v\tau_{zy})}{\partial z} + \frac{\partial(w\tau_{xz})}{\partial x} + \frac{\partial(w\tau_{yz})}{\partial y} + \frac{\partial(w\tau_{zz})}{\partial z} + div(k grad T) + S_E \right]$$

D. Kappa-Epsilon model

K – Equation

$$\rho \left[ \bar{u} \frac{\partial k}{\partial x} + \bar{v} \frac{\partial k}{\partial r} \right] = \frac{\partial}{\partial x} \left[ (\mu_t + \frac{\mu_t}{\sigma_k}) \frac{\partial k}{\partial x} \right] + \frac{1}{r} \frac{\partial}{\partial r} \left[ r (\mu_t + \frac{\mu_t}{\sigma_k}) \frac{\partial k}{\partial r} \right] + \frac{\rho g}{\rho \varepsilon} - \frac{\rho \cdot U_0 \cdot D_h}{\mu}$$

Where, G is the production term and is given by

G=

$$\mu_t \left[ 2 \left\{ \left( \frac{\partial \bar{v}}{\partial r} \right)^2 + \left( \frac{\partial \bar{u}}{\partial x} \right)^2 + \left( \frac{\bar{v}}{r} \right)^2 \right\} + \left( \frac{\partial \bar{u}}{\partial r} + \frac{\partial \bar{v}}{\partial x} \right)^2 \right]$$

ε - Equation

$$\rho \left[ \bar{u} \frac{\partial \varepsilon}{\partial x} + \bar{v} \frac{\partial \varepsilon}{\partial r} \right] = \frac{\partial}{\partial x} \left[ (\mu_t + \frac{\mu_t}{\sigma_\varepsilon}) \frac{\partial \varepsilon}{\partial x} \right] + \frac{1}{r} \frac{\partial}{\partial r} \left[ r (\mu_t + \frac{\mu_t}{\sigma_\varepsilon}) \frac{\partial \varepsilon}{\partial r} \right] + C_{s1} G \frac{\varepsilon}{k} - C_{s2} \frac{\varepsilon^2}{k}$$

Here  $C_{s1}$ ,  $C_{s2}$ ,  $\sigma_k$  and  $\sigma_\varepsilon$  are the empirical turbulent constant. The values of  $C_\mu$ ,  $C_{s1}$ ,  $C_{s2}$ ,  $\sigma_k$  and  $\sigma_\varepsilon$  are 0.09, 1.44, 1.92, 1.0 and 1.3 respectively.

E. Boundary Conditions

Fluid flow is considered to be turbulent. The quantities  $U$ ,  $k$ , are obtained by using numerical calculations based on the  $k$ - model for high Reynolds Number. The boundary conditions are listed below:

1) At the inlet of the channel

$$u = U_{in}, v = 0$$

$$k_{in} = 0.005 U_{in}^2$$

$$\varepsilon_{in} = 0.1 K_{in}^2$$

$K_{in}$  stands for the admission condition for turbulent kinetic energy and  $\varepsilon_{in}$  is the inlet condition for dissipation.

2) At the walls:

$$u = v = 0$$

$$k = \varepsilon = 0$$

3) At the exit:

$$P = P_{atm}$$

The Reynolds number based on circular diameter in case of circular tube and hydraulic diameter  $D_h$  in case of rectangular tube, parallel plates.

#### IV. SOLUTION PROCEDURE

The time-independent incompressible Navier–Stokes equations and the turbulence model were discretized using the finite volume method. Second order upwind scheme was applied for convective and turbulent terms. To evaluate the pressure field, the pressure–velocity coupling algorithm SIMPLE (Semi Implicit Method for Pressure-Linked Equations) was selected. At the inlet, uniform velocity profile has been imposed. Impermeable boundary condition has been implemented over the channel wall while constant heat flux condition is applied to the lower wall of test section. The turbulence intensity was kept at 10% at the inlet. Two parameters of interest for present case are: (1) Nusselt Number (2) friction factor. The friction factor,  $f$  is computed by pressure drop,  $p$  across the length of test section,  $L$ , having the hydraulic diameter,  $D_h=2H$  as

$$f = \frac{\Delta p}{4 \left( \frac{L}{D_h} \right) \frac{\rho u^2}{2}}$$

The heat transfer is measured by Nusselt number which can be obtained by

$$Nu = \frac{h}{k/D_h}$$

#### V. RESULTS

The results for smooth plate are calculated according to the correlation use by Lorenz et.al. [6], figure 4. shows the heat transfer results for air ( $T_i=299$  K) flow in the channel for three different rib width ratios ( $B/H=0.5, 0.75, 1$ ). In the figure, the Nusselt number are related as a function of Reynolds number. The results for smooth channel is also presented in the figure for comparison. It is shown that the Nusselt number increases with increase in Reynolds number. In all cases, ribbed channel flow gives higher value for Nusselt number than that for smooth channel flow due to induced turbulence. The maximum Nusselt number is obtained for  $B/H=0.75$ .

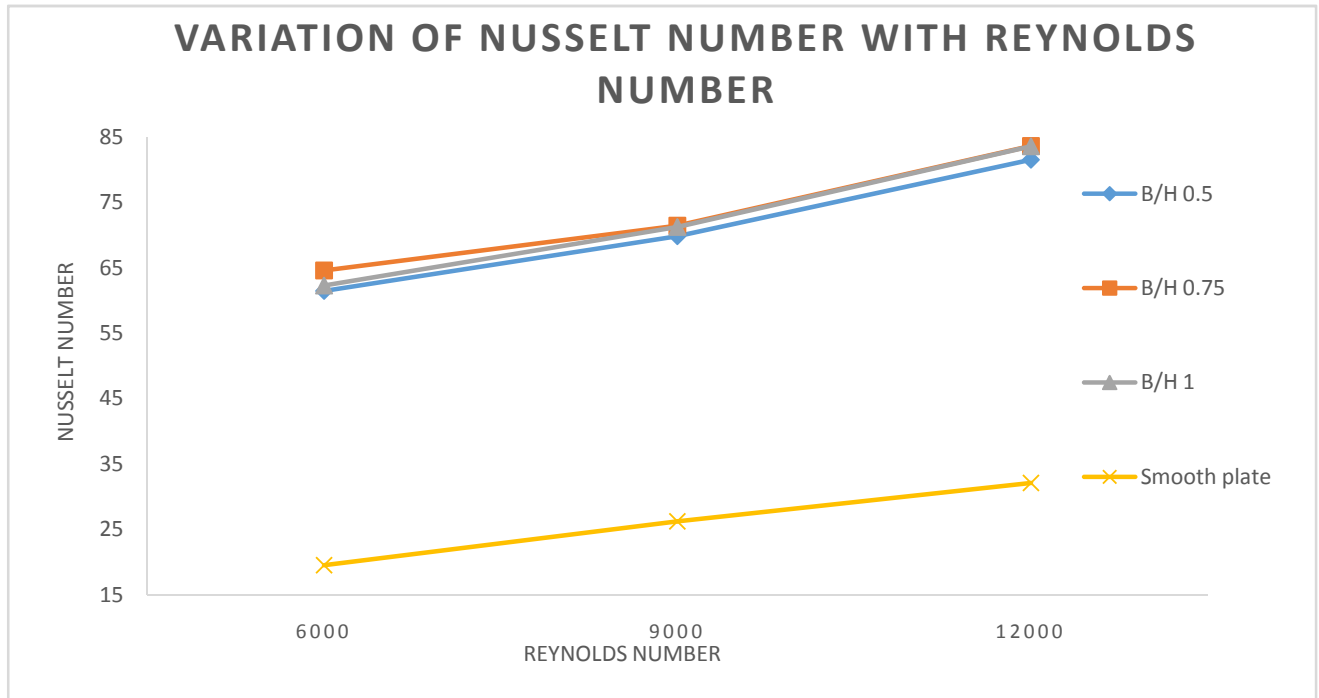


**Fig. 4.** Variation of Nusselt number with Reynolds number.

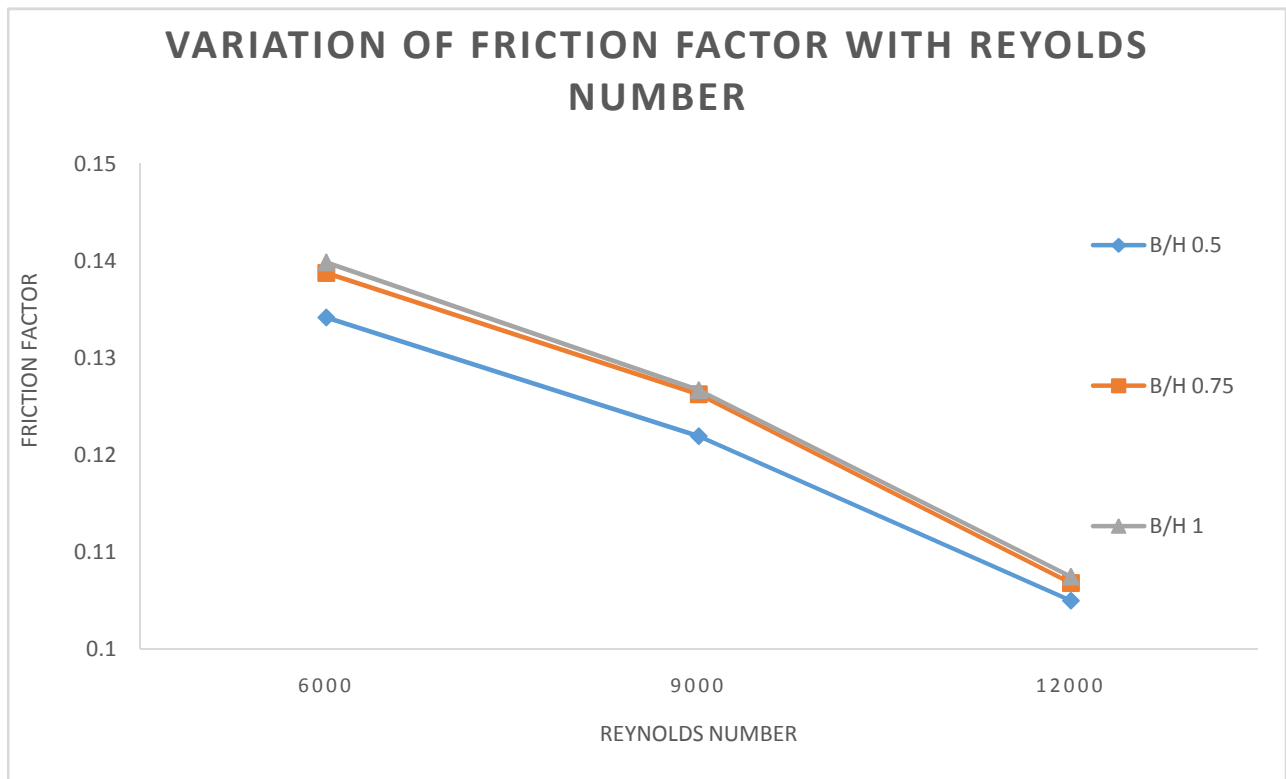
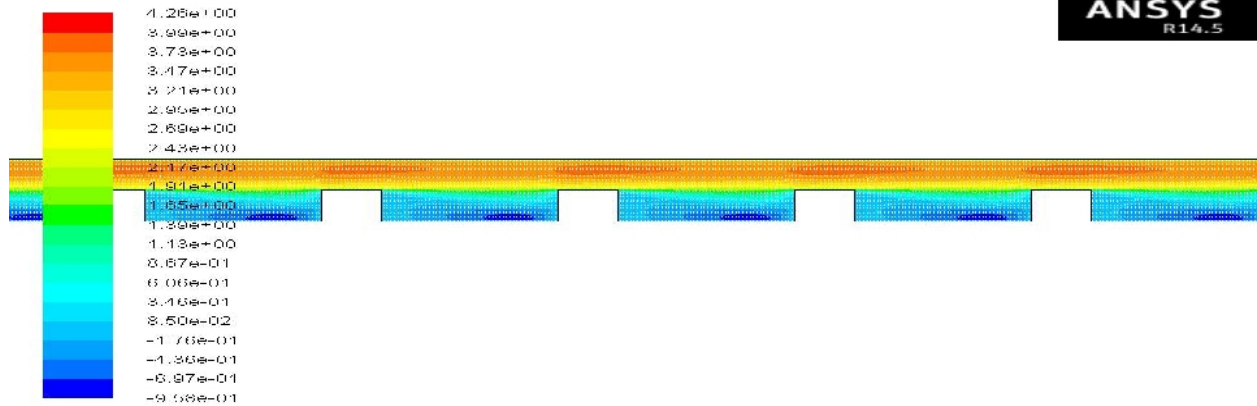
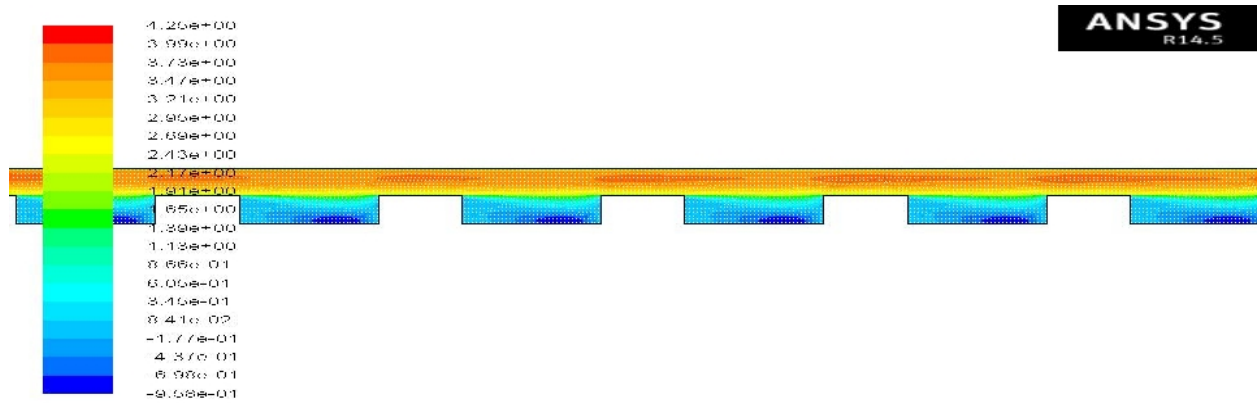


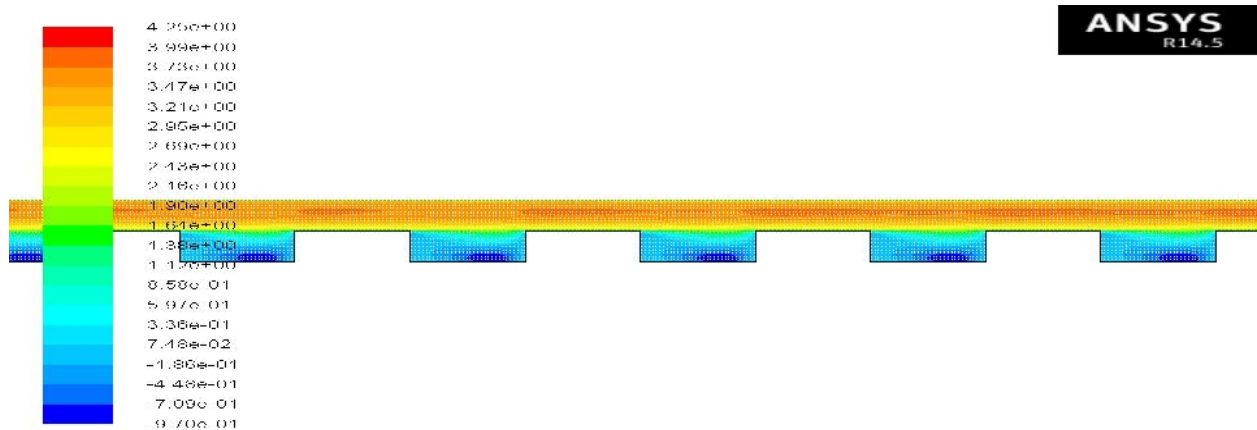
**Fig. 5.** Variation of Friction factor with Reynolds number.



X-Velocity for B/H 0.5



X-Velocity for B/H 0.75



X-Velocity for B/H 1

The increase in Nusselt number values by using different ratios of B/H are about 143% to 216%. Figure 5. shows results for friction factor for different B/H ratios. It is observed that the friction factor decreases with increase in Reynolds number in all cases due to increase in pressure drop. Maximum friction factor is found for B/H 1.

Contours of X-velocity at Reynolds number 9000 are also provided in above figures showing the recirculation zone for different B/H ratios. It is observed that with increase in B/H ratio there is decrease in recirculation zone. But the velocity of fluid in recirculation zone is nearly same for all three B/H ratio.

## VII. CONCLUSION

Numerical investigation of forced convection in a two-dimensional turbulent channel with periodic transverse ribs on the lower channel for examining heat transfer and friction factor is performed. It is found that Nusselt number increases about 143% to 216% by use of ribbed protrusion, and maximum enhancement is shown by B/H 0.75 with an increment of 149%, 160% and 216% for respective Reynolds number, the increment is about 6% to 15% when compared to other two B/H ratio.

## REFERENCE

- [1]. Bhola, M., Singh, S., 2015, "Analysis of Heat Transfer in Turbulent Channel Using Grooves", *International Journal of Science and Research*, **4**, 5, 2857-2871
- [2]. Chaube, A., Sahoo, P.K., Solanki, S.C., 2006, "Analysis of Heat Transfer Augmentation and Flow Characteristics Due to Rib Roughness Over Absorber Plate of a Solar Air Heater", *Renewable Energy*, **31**, 317-331
- [3]. Deylami, H.M., Amanifard, N., Sanaei, M., Kouhikamali, R., 2013, "Numerical Investigation of Heat Transfer and Pressure Drop in a Corrugated Channel", *International Journal of Engineering*, **26**, 7, 771-780
- [4]. Eiamsa-ard, S., Promvong, P., 2008, "Numerical Study on Heat Transfer of Turbulent Channel Flow Over Periodic Grooves", *International Communications in Heat and Mass Transfer*, **35**, 844-852
- [5]. Kumar Manoj and Agarwal Ashish, 2014, "Analysis of Heat Transfer Augmentation And Flow Characteristics Due to Rib Roughness of a Solar Air Heater", *International Journal of Emerging Technologies in computational and Applied Science*, **8**, 249-252.
- [6]. Lorenz, S., Mukomilow, D., Leiner, W., 1995, "Distribution of the Heat Transfer Coefficient in a Channel with Periodic Transverse Grooves", *Experimental Thermal and Fluid Sciences*, **11**, 234-242.
- [7]. Luo, D.D., Leung, C.W., and Chan, T.L., 2004, "Forced Convection and Flow Friction Characteristics of Air-Cooled Horizontal Equilateral Triangular Ducts with Ribbed Internal Surfaces", *International Journal of Heat and Mass Transfer*, **47**, 5439-5450.
- [8]. Mashilkar, B.B. and Varkute Nilesh, 2014, "Numerical Investigation of Heat Transfer Augmentation in a Rectangular Solar Air Heater Duct", *International Journal of Engineering Research and Technology*, **3**, 1245-1248
- [9]. Sahu, R.K. and Gandhi, B.K., 2014, "Numerical Simulation of Heat Transfer Enhancement Due to a Gap in an Inclined Continuous Rib Arrangement in a Solar Air Heater Duct", *International Journal of Advanced Mechanical Engineering*, **4**, 687-693
- [10]. Singh Dharam and Bartaria, V.N., 2013, "CFD Study on Heat Transfer Through Solar Air Heater Absorber Plate with Surface Roughness", *International journal of Engineering Business and Enterprise Applications*, **6**, 51-55
- [11]. Singh, A.P. and Singh, N.K., 2014, "Numerical Analysis of Heat Transfer in Turbulent Channel Flow with Longitudinal Vortex Generators", *International Journal of Research in Management, Science and Technology*, **2**, 43-51
- [12]. Sohankar, A., 2010, "Heat Transfer and Fluid Flow Through a Ribbed Passage in Staggered Arrangement", *Iranian Journal of Science and Technology, Transaction B: Engineering*, **34**, 471-485
- [13]. Tatsumi, K., Iwai, H. and Inaoka, K., 2002, "Numerical Simulation for Heat and Fluid Characteristics of Square Duct with Discrete Rib Turbulators", *International Journal of Heat and Mass Transfer*, **45**, 4353-4359
- [14]. Vijiapurapu Sowjanya and Cui Jie, 2007, "Simulation of Turbulent Flow in a Ribbed Pipe Using Large Eddy Simulation", *Numerical Heat Transfer, Part A: Applications: An International Journal of Computation and Methodology*, **51**, 1137-1165.